High-pressure transition to the post-barite phase in BaCrO$_4$ hashemite

D. Santamaría-Pérez,[1,*] Ravhi S. Kumar,[2] A. J. Dos santos-García,[3] D. Errandonea,[4] R. Chuliá-Jordán,[1] R. Saez-Puche,[3]
P. Rodríguez-Hernández,[5] and A. Muñoz[5]

[1]*Departamento de Química Física I, MALTA Consolider Team, Universidad Complutense de Madrid,*
Avenida Complutense s/n, 28040 Madrid, Spain

[2]*High Pressure Science and Engineering Center, Department of Physics and Astronomy, University of Nevada–Las Vegas,*
4505 Maryland Parkway, Las Vegas, Nevada 89154-4002, USA

[3]*Departamento de Química Inorgánica, Universidad Complutense de Madrid, Avenida Complutense s/n, 28040 Madrid, Spain*

[4]*Departamento de Fisica Aplicada, ICMUV, Universitat de Valencia, MALTA Consolider Team, Edificio de Investigación, C. Dr. Moliner 50,*
Burjassot, 46100 Valencia, Spain

[5]*Departamento de Física Fundamental II, MALTA Consolider Team, Universidad de La Laguna, La Laguna, Tenerife, Spain*

A recent high-pressure study on barium chromate BaCrO$_4$ reported a phase transition but the structure of the high-pressure phase structure could not be identified. This high-pressure phase was suggested to have a monoclinic structure different from other high-pressure forms of ABO$_4$-type compounds. In this work, we have carried out x-ray diffraction measurements up to 46 GPa using He as the quasihydrostatic pressure medium and density-functional theory calculations. Our studies allow us to identify the high-pressure phase as the $P2_12_12_1$ post-barite-type phase, recently reported for BaSO$_4$. The equations of state of both, the low- and the high-pressure phases have been determined. Elastic constants of the initial barite-type phase were calculated and the shear and Young moduli, and the Poisson coefficient deduced from them. Finally Raman and infrared-active modes are also calculated, discussed, and compared with experiments when possible. As a first approximation, the vibrations can be separated in internal vibrations of the CrO$_4$ tetrahedra and vibrations where the tetrahedral units behave as rigid units. Pressure coefficients of the different modes are reported being two soft modes found for the high-pressure phase.

I. INTRODUCTION

Minerals of the barite-type family are of great interest for Earth[1] and material sciences.[2–4] This family includes some ABO$_4$ sulphates, chromates, phosphates, and perclorates, amongst others, which crystallize in an orthorhombic structure [space group (S.G.) *Pnma*]. Its structure has been usually described in terms of oxygen polyhedra, the oxide being formed by isolated [BO$_4$] tetrahedra and complex [AO$_{12}$] dodecahedra, but a more recent description in terms of its AB cation subarray provides a different point of view, showing the similarity between the AB sublattice in the ternary oxide and the structure of the FeB alloy [see Fig. 1(a)]. A more detailed analysis of this structure type can be found in Refs. 5–7. Many ternary halides adopt this structure as well.

On the other hand, compounds adopting this type of structure have been of renewed interest regarding their high-pressure (HP) behavior.[6,8–11] Although experimental evidence of post-barite transitions are known since the pioneering work of Bridgman,[12] the structural determination of the post-barite phase could not be achieved until last year. Santamaría-Pérez *et al.* found that barite transforms into another orthorhombic structure [S.G. $P2_12_12_1$, Fig. 1(b)], with no change in the coordination number of A or B atoms ([BO$_4$] tetrahedra and [AO$_{12}$] dodecahedra).[11] However, the second coordination sphere of the A/B atoms presents an increase of neighboring atoms from 7 to 8; i.e., the cation subarray AB of the post-barite structure can be considered as an intermediate framework between the FeB-type (corresponding to the initial *Pnma* barite structure) and the CsCl-type structures.[6] Additionally, Errandonea and co-workers have recently proposed a monoclinic

$P2_1/m$ structure for a HP post-barite phase in AgClO$_4$, which also presents an AB sublattice closely related to the CsCl-type structure.[13]

The determination of the post-barite phase has allowed completion of the lower right quadrant of the Bastide diagram which, based on the relative cation sizes, provides systematic trends in phase transitions in ABO$_4$ isotypes.[14] Thus, the northeast phase-transition rule predicts that compounds with the monazite-type structure would transform upon compression either to the scheelite or the barite structure. For instance, the latter behavior was observed in the phosphate LaPO$_4$ (Ref. 15) and in the sulphate CaSO$_4$ at high pressures.[16,17] Therefore, post-barite could be a potential structure for both the monazite- and the barite-type structures at high pressures.

Thus, intrigued by the recent report of a high-pressure phase transition in the barite-type BaCrO$_4$ compound (mineral name, hashemite) at about 10 GPa, where no structural determination could be done,[9] we have reinvestigated the high-pressure behavior of barium chromate by means of angle-dispersive x-ray diffraction (ADXRD) measurements using He as a pressure medium. The experiments allow identifying the orthorhombic post-barite phase previously found in BaSO$_4$ under compression. Our results are supported by total-energy *ab initio* calculations.

II. EXPERIMENTAL AND THEORETICAL METHODS

A. Experimental details

Polycrystalline BaCrO$_4$ powder was prepared via the traditional solid-state reaction. Predried stoichiometric amounts of
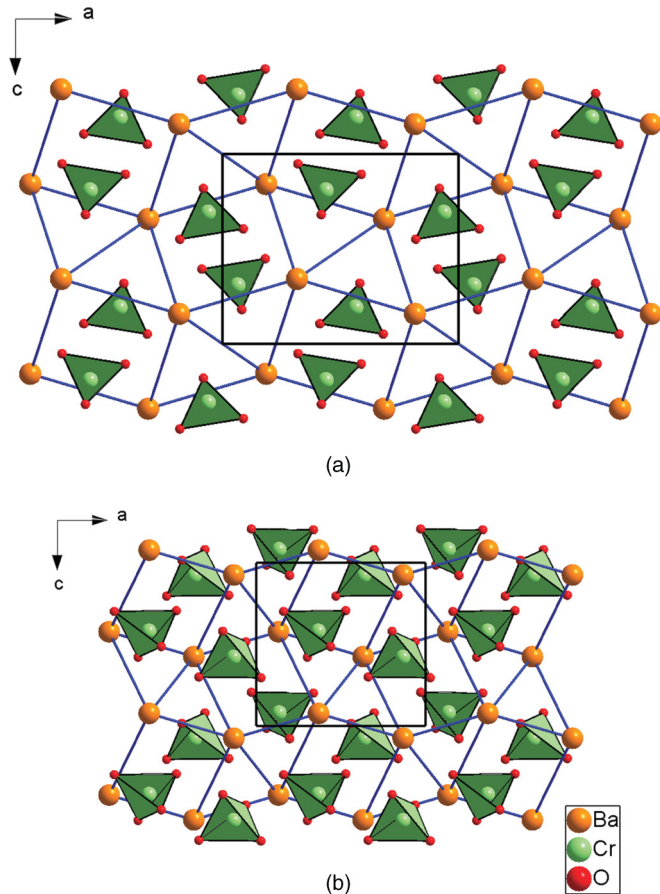
FIG. 1. (Color online) (a) Barite-type structure of $BaCrO_4$ at room conditions projected onto the *ac* plane. Orange and green and tiny red circles represent Ba, Cr, and O atoms, respectively. (b) Structure of the high-pressure phase of $BaCrO_4$ at 45.9 GPa projected also on the same plane.

Cr_2O_3 and $BaCO_3$ (>99%, Aldrich) were intimately ground in acetone and then fired at 850 °C for 16 h. The resulting powder was ground again and pressed uniaxially into pellets at 1 metric ton. The pellets were then fired at 950 °C for 36 h. The x-ray diffraction pattern at ambient pressure (AP) confirmed the barite-type structure.

High-pressure ADXRD experiments were carried out up to 46 GPa at the 16-IDB beamline of the HPCAT at the Advanced Photon Source (APS). We used an incident monochromatic wavelength of 0.37379 Å focused down to 10 μm × 10 μm. Measurements were performed in a symmetric diamond-anvil cell (DAC) with diamond cutlets of 300 μm and a drilled rhenium gasket (100-μm-diameter hole). The diffraction patterns were recorded on a MAR345 image plate located 350 mm from the sample. Barium chromate powder was loaded in the diamond-anvil cell using helium (He) as the pressure-transmitting medium to guarantee quasihydrostatic conditions in almost the whole pressure range covered by the experiments. Detector calibration, correction of distortion, and integration to conventional 2θ-intensity data were carried out with the FIT2D software.[18] In this study the pressure was determined using the ruby fluorescence technique.[19] The indexing and refinement of the powder patterns were performed using the FULLPROF[20] and POWDERCELL[21] program packages.

B. Calculation details

We have performed *ab initio* total-energy calculations within the density-functional theory (DFT)[22] using the plane-wave method and the pseudopotential theory with the Vienna *ab initio* simulation package (VASP).[23–26] We have used the projector-augmented wave scheme (PAW)[27,28] implemented in this package to take into account the full nodal character of the all-electron charge density in the core region. Basis sets including plane waves up to an energy cutoff of 520 eV were used in order to achieve highly converged results and an accurate description of the electronic properties. The description of the exchange-correlation energy was performed with the generalized gradient approximation (GGA) with the PBEsol prescription.[29] A dense special *k*-point sampling for the Brillouin zone (BZ) integration was performed in order to obtain very well converged energies and forces. At each selected volume, the structures were fully relaxed to their equilibrium configuration through the calculation of the forces and the stress tensor. In the relaxed equilibrium configuration, the forces on the atoms are less than 0.006 eV/Å and the deviation of the stress tensor from a diagonal hydrostatic form is less than 1 kbar (0.1 GPa). From our results we obtain the *E-V* third-order Birch-Murnaghan equation of state (EOS) that can be fitted using a standard fitting procedure in order to obtain the bulk modulus and its pressure derivative. We also obtain the relative stability of the different analyzed structures. Our study is a $T = 0$ K (zero-point effects are not included). A phase transition occurs in our study when two phases have the same enthalpy ($E_1 + P_t V_1 = E_2 + P_t V_2$). This allows us to obtain the theoretical transition pressure under these conditions. The application of DFT-based total-energy calculations to the study of semiconductor properties under high pressure has been reviewed in Ref. 30, showing that the phase stability, electronic, and dynamical properties of compounds under pressure are well described by DFT.

We have also performed lattice dynamics calculations of the phonons at the zone center (Γ point) of the BZ. Our theoretical results enable us to assign the Raman modes observed for the different phases. Furthermore, the calculations provide information about the symmetry of the modes and polarization vectors. Highly converged results on forces are required for the calculation of the dynamical matrix. We use the direct force constant approach (or supercell method).[31] The construction of the dynamical matrix at the Γ point of the BZ is particularly simple and involves separate calculations of the forces in which a fixed displacement from the equilibrium configuration of the atoms within the *primitive* unit cell is considered. Symmetry aids by reducing the number of such independent displacements, reducing the computational effort in the study of the analyzed structures considered in this work. Diagonalization of the dynamical matrix provides both the frequencies of the normal modes and their polarization vectors. This allows us to identify the irreducible representation and the character of the phonon modes at the Γ point.

Mechanical stability of homogeneous crystals is an interesting subject that can provide important information concerning the study of the structural transformations via the stability criteria related with the mechanical properties. Knowledge of the elastic behavior can be essential for many

practical applications. These elastic constants can be obtained computing the macroscopic stress after the application of a small strain by using the stress theorem.[32] Alternatively, it can also be calculated using density-functional perturbation theory (DFPT).[33] For the evaluation of the elastic constants, first we obtain the ground state relaxed structure, and later the structure was strained in different directions according to their symmetry in order to obtain the elastic constants. The total-energy variations were evaluated according to a Taylor expansion[34] for the total energy with respect to the applied strain. Due to this fact it is important to check that the strain used in the calculations guarantees the harmonic behavior. This allows us to obtain the C_{ij} elastic constants in the Voigt notation and the number of independent elastic constants is reduced completely by crystalline symmetry.[35]

III. RESULTS AND DISCUSSION

Figure 2 shows a selection of our ADXRD data for BaCrO$_4$ collected at several selected pressures with He as the pressure medium. It is necessary to point out that the crystal sizes of our powdered sample are not uniform and, consequently, some texturing effects appear in the x-ray diffraction patterns. This unwanted effect entails that the relative intensities of the diffraction maxima are not accurate, affecting the quality of structural refinements. At ambient conditions, the x-ray diffraction pattern corresponds to the orthorhombic barite-type
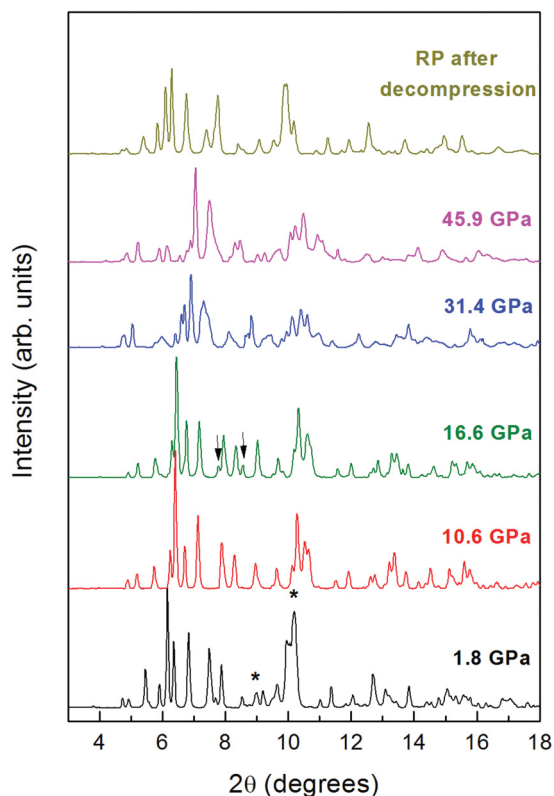

FIG. 2. (Color online) Powder x-ray diffraction patterns of BaCrO$_4$ at increasing pressure conditions using He as the pressure-transmitting medium. Black arrows indicate the appearance of new peaks and asterisks denote the diffraction maxima of Re (gasket material).

structure previously reported (S.G. *Pnma*)[36,37] with similar lattice parameters: $a = 9.1165(6)$ Å, $b = 5.5264(4)$ and $c = 7.3347(5)$ Å [$V = 369.5(1)$ Å^3] (see Table I). The high-pressure XRD patterns could be indexed in the initial *Pnma* phase up to 13.6 GPa. Upon further compression additional diffraction peaks appear (arrows in the diffraction patterns at 16.6 GPa), which indicates the onset of a phase transition in BaCrO$_4$. In parallel, the intensity of the peaks of the low-pressure phase gradually decreases. This transition pressure is considerably higher than the 9.8 GPa reported by Huang *et al.* using a 4:1 methanol-ethanol mixture as the pressure-transmitting medium.[9] Thus, the lack of hydrostaticity drives the onset of the phase transition to occur at lower pressures, as has also been observed in other compounds,[38,39] in particular, in isomorphic BaSO$_4$.[11]

The variation of the volume [Fig. 3(a)] and lattice parameters [Fig. 3(b)] of the initial phase with pressure was obtained from the present data. The pressure-volume curves were analyzed using a third-order Birch-Murnaghan EOS. By fixing the zero-pressure volume (V_0) to its measured value, we obtained the bulk modulus (B_0) and its pressure derivative (B_0'), which are collected in Table II. The experimental values of these characteristic parameters are also in good agreement with those obtained from *ab initio* calculations (see Table II). As can be seen in Fig. 3(b), the contraction of the lattice parameters is rather anisotropic. For instance, according to our experiments, the relative contractions for a, b, and c between room pressure and 16.6 GPa are 4.33, 6.96, and 7.29%, respectively. These values are also in good agreement with those from theoretical simulations, where a, b, and c axes decrease 4.01, 7.2, and 7.52%, respectively, in this pressure range. Additionally, the evolution of the different axes can be described by a second-order polynomial function: $a(\text{Å}) = 9.114(5) - 0.036(2)P + 7.5(9) \times 10^{-4}P^2$, $b(\text{Å}) = 5.517(7) - 0.041(2)P + 11(1) \times 10^{-4}P^2$, and $c(\text{Å}) = 7.333(5) - 0.044(2)P + 7.0(8) \times 10^{-4}P^2$, where the pressure P is in GPa. Results are in good agreement with Huang's data[9] below 7.2 GPa but, at higher pressures, our data shows a slightly larger compressibility of the lattice parameters [see Figs. 3(a) and 3(b)]. This fact entails that the B_0' value obtained by Huang *et al.* is considerably large ($B_{0,\text{Huang}}' = 6.8$), which evidences the existence of nonhydrostatic effects above this pressure. Note also, that the compressibility of barium chromate is slightly higher than that of barite itself (BaSO$_4$), where the bulk modulus and its first pressure derivative are $B_0 = 58.6$ GPa and $B_0' = 4.8$.

From this observation, assuming that the [BaO$_{12}$] polyhedra are equally compressible in both compounds, it can be inferred that the volume of the [CrO$_4$] tetrahedral units decrease more rapidly with pressure than that of the [SO$_4$] units. Furthermore, the compressibility of the ACrO$_4$ structures is intimately related with that of the A-centered oxygen polyhedra. In other words, the A-O bonds are usually by far the most compressible. The bulk moduli of chromates with divalent A cations seem to depend on both the average A-O distance (d in Angstroms) in this polyhedra and the coordination number of the A atom (CN$_A$). Thus, the experiential criterion, $B_0(\text{GPa}) = 286(16) - 109(8)d^3/\text{CN}_A$ would explain the bulk moduli of the barite-type BaCrO$_4$ (54 GPa), the monazite-type PbCrO$_4$ (57 GPa),[40] and the zircon-type CaCrO$_4$ (104 GPa)[41] structures. Additional

TABLE I. Experimental and calculated GGA lattice parameters, volumes, and fractional coordinates of room-pressure *Pnma* barite-type phase and the high-pressure $P2_12_12_1$ post-barite-type phase. The experimental lattice parameters of the barite-type phase correspond to the indexation of our XRD pattern, but the atomic coordinates are those reported in Ref. 37.

		RP barite-type *Pnma* phase		HP post-barite-type $P2_12_12_1$ phase	
		Experimental	Theoretical	Experimental (27.4 GPa)	Theoretical (27.9 GPa)
a (Å)		9.1165(6)	9.0889	6.860(1)	6.7839
b (Å)		5.5264(4)	5.5021	6.1602(8)	6.1676
c (Å)		7.3347(5)	7.3188	6.5351(8)	6.4965
V (Å^3)		369.5(1)	366.0	276.2(4)	271.8
	x	0.1830	0.1837		0.6356
Ba	y	0.25	0.25		0.3022
	z	0.1553	0.1547		0.5767
	x	0.5574	0.5572		0.6369
Cr	y	0.25	0.25		0.2273
	z	0.8057	0.8051		0.0772
	x	0.3900	0.3876		0.4573
O$_1$	y	0.25	0.25		0.1348
	z	0.8837	0.8827		0.2179
	x	0.6792	0.6812		0.8331
O$_2$	y	0.25	0.25		0.2987
	z	0.9676	0.9689		0.2094
	x	0.5847	0.5819		0.4322
O$_3$	y	0.0113	0.0060		0.9492
	z	0.6777	0.6757		0.5366
	x				0.6975
O$_4$	y				0.0443
	z				0.9055

measurements of the bulk moduli of chromates are necessary to validate such a relationship.

Above 16.6 GPa, the XRD patterns could be indexed using two different phases:

(i) a *Pnma* barite-type structure, similar to the initial structure, except for the sudden small change in the *b* and *c* lattice parameters at this pressure. The *b* axis contracts ∼3.3%, the *c* axis expands ∼0.6%, and the *a* axis remains nearly constant between 16.6 and 19.6 GPa, with the volume decreasing in a continuous way [see Figs. 3(a) and 3(b)]; and

(ii) a different orthorhombic structure whose structural model could correspond to the HP phase found in barite,[11] S.G. $P2_12_12_1$. This post-barite phase was also recently found in CeVO$_4$ under compression.[42] The indexation of this high-pressure phase could be only performed above 27.4 GPa using ten diffraction lines that were not explained by the barite-type phase (see in the inset of Fig. 4 the limited quality of the data above 30 GPa). Attempts to index the lines of the diagrams upon compression between 16.6 and 27.4 GPa were unsuccessful, suggesting that the extra peaks in fact

TABLE II. Experimental, theoretical (from EOS), and previously reported unit-cell volumes at zero pressure (V_0), bulk moduli (B_0), and the first derivatives with pressure (B'_0) of both, the low-pressure barite-type and the high-pressure post-barite-type phases. Transition pressures are also indicated. In the HP phase (only five data points), the B'_0 value was fixed to 4.5 to avoid physically meaningless results.

|	EOS	Transition pressure (GPa)	V_0 (Å^3)	B_0 (GPa)	B'_0
Low-pressure barite-type phase (S.G. *Pnma*)	Experimental (this work)	∼15	369.5(1)	53.3(9)	4.6(2)
	Theoretical (this work)	14.9	365.7(3)	56.0(8)	4.3(1)
	Experimental (Ref. 9)	9.8	369.9(2)	53(1)	6.8(5)
	Theoretical (Ref. 43)		370.6	56.05	
High-pressure post-barite-type phase (S.G. $P2_12_12_1$)	Experimental (this work)		365(8)	53(6)	4.5 (fixed)
	Theoretical (this work)		370(2)	36(2)	6.0(2)
			355(1)	57(1)	4.5 (fixed)
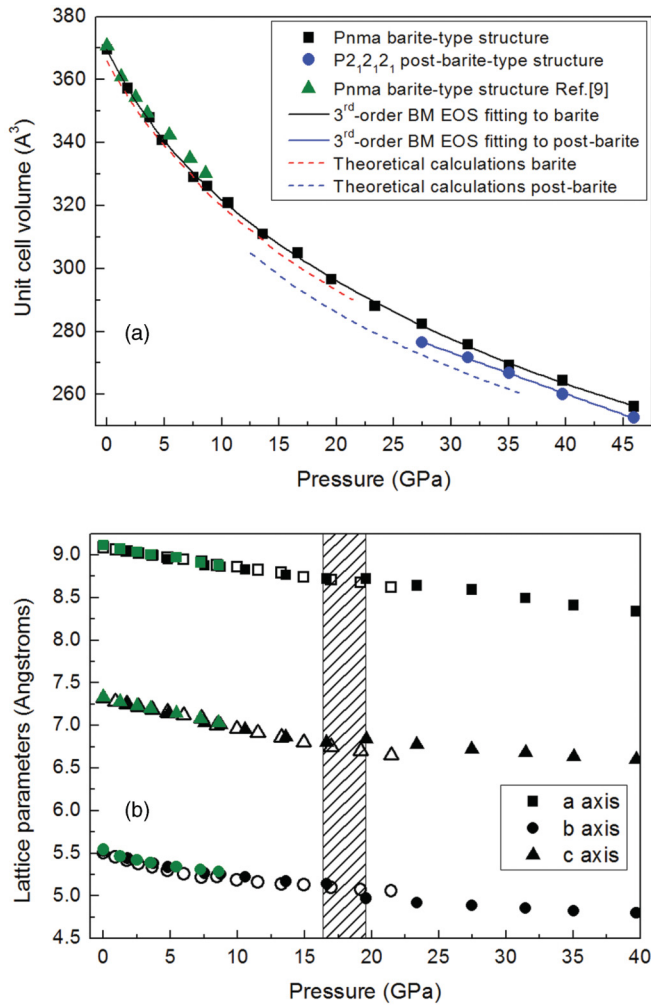
FIG. 3. (Color online) (a) Experimental and calculated pressure dependence of the unit-cell volume for the two phases of BaCrO$_4$. Black squares (red dashed line) and blue circles (blue dashed line) correspond to the experimental (calculated) data for the barite-type and the post-barite-type phases. (b) Evolution of the lattice parameters of the LP barite-type phase with pressure. Squares, circles, and triangles represent the a, b, and c axes. Black solid and empty symbols correspond to experiments and calculations, respectively. Green symbols correspond to experimental results reported in Ref. 9. The shadowed region indicates the small discontinuity in lattice constants.

correspond to one or several polymorphs with intermediate structures. We have also examined the monazite-type, the AgMnO$_4$-type, and the monoclinic $P2_1/m$ unit cell proposed by Huang and co-workers,[9] but their diffraction peak positions failed to match the HP phase.

The slowness of the phase transition to the $P2_12_12_1$ post-barite structure becomes apparent in the wide pressure range of phase coexistence. The LeBail fit of the XRD pattern at 45.9 GPa depicted in Fig. 4 illustrates the quality of the indexation. It is also important to remark that, despite the texturing effects of the XRD patterns, the relative intensity of the Bragg peaks of the high-pressure phase is not far from that predicted for the $P2_12_12_1$ post-barite structural model. A tentative estimation of the relative fraction of the HP phase at this pressure gives a value of circa 64%. This
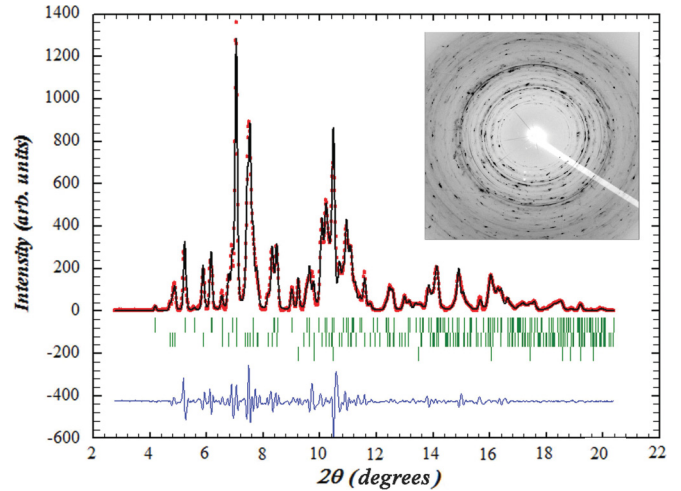

FIG. 4. (Color online) LeBail refinement of the x-ray diffraction pattern of BaCrO$_4$ at 45.9 GPa. Observed, calculated, and difference profiles are represented as black, red, and blue lines. Vertical markers indicate Bragg reflections of the *Pnma* barite-type (top), $P2_12_12_1$ post-barite-type (center) structures, and the rhenium gasket (bottom).

phase transition would imply a volume collapse of ~1.2%. The compression of the high-pressure $P2_12_12_1$ phase seems to also be highly anisotropic. In particular, the b axis is quite incompressible with only a variation of 1% between 27.4 and 45.9 GPa, whereas the a and c axes decrease 4.6 and 3.2%, respectively. Rough parameters of the tentative experimental EOS are collected in Table II and show that the high-pressure phase would exhibit a similar compressibility to that of the initial barite-type phase and very different from that estimated by Huang *et al.*[9] for the HP phase using the tentative $P2_1/m$ unit cell ($B_0 = 117$ GPa and $B'_0 = 3$). The similarity of the bulk moduli can be explained by the fact that, in both structures, the coordination sphere of the Ba and Cr atoms ([BaO$_{12}$] dodecahedra and [CrO$_4$] tetrahedra) would not change significantly at the transition. It is also important to remark that, as can be seen in Fig. 2, the phase transition is reversible; i.e., the initial barite-type structure is fully recovered after decompression.

These experimental observations are supported by *ab initio* total-energy calculations. According to calculations the barite structure is the thermodynamically stable phase at ambient pressure. As can be seen in Table I, the calculated lattice parameters and fractional coordinates compare very well to those from our experiment and previous reported data,[36,37] the unit-cell volume being only slightly underestimated (<1%). In Fig. 5, it can be clearly seen that the theoretical energy-volume curves of the initial barite-type and the HP $P2_12_12_1$ post-barite-type phases cross each other at high pressure. As shown in the enthalpy difference as a function of pressure plot (Fig. 5, inset), the HP phase becomes more stable than the barite-type phase at 14.9 GPa. According to the calculations, this transformation entails a volume change of 2.2%, which is in relatively good agreement with the experimental results. The calculated fractional coordinates of this HP phase are in good agreement with those of the experimental post-barite structure reported for HP-BaSO$_4$ (see Table I and Ref. 11). The calculated EOS parameters collected in Table II also
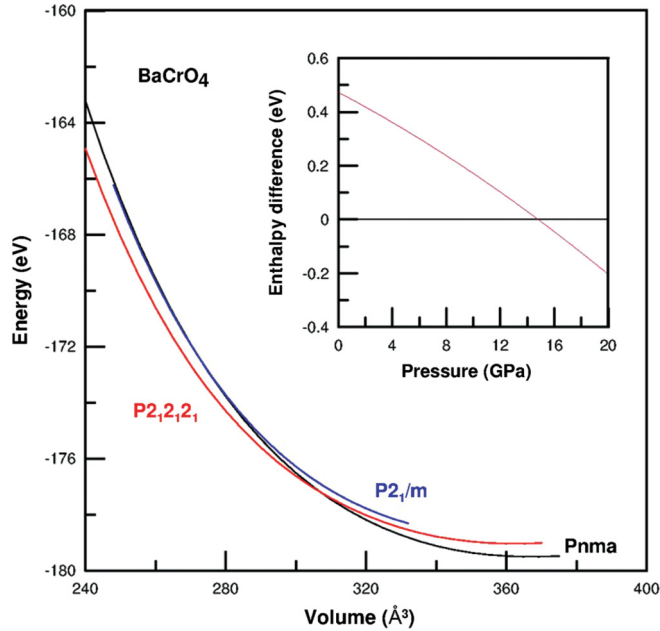
FIG. 5. (Color online) Internal energy as a function of volume for the *Pnma* barite-type structure and the $P2_12_12_1$ post-barite-type structure of BaCrO$_4$. The $P2_1/m$ (S.G. 11) structure proposed by Errandonea *et al.* for a high-pressure phase of AgClO$_4$ is also included (Ref. 13). Inset: Enthalpy variation versus pressure.

TABLE III. Computed elastic constants of BaCrO$_4$-hashemite of the present work (GPa) compared with those previously reported and with the experimental ones corresponding to BaSO$_4$.

	BaCrO$_4$ Theoretical (this work)	BaCrO$_4$ Theoretical (Ref. 43)	BaSO$_4$ Experimental (Ref. 44)
C_{11}	106.9	102.5	88.3
C_{22}	71.8	92.6	78.1
C_{33}	101.8	111.7	103.8
C_{44}	5.5	12.5	11.7
C_{55}	35.6	35.5	28
C_{66}	17.2	23.9	25.5
C_{12}	32.4	38.1	47.7
C_{13}	29.7	32.3	28.9
C_{23}	24.3	29.3	26.9

agree well with those estimated experimentally, as can also be deduced by looking at the theoretical and experimental evolution of the lattice volumes with pressure in Fig. 3(a). It is also important to mention that the small discontinuity in the evolution of the lattice parameters with pressure observed experimentally between 16.5 and 19.4 GPa was not reproduced by the calculations, where the unit-cell axes decrease smoothly. The nature of this anomalous behavior is not yet understood.

Figure 5 also shows the calculated total energy for a potential post-barite $P2_1/m$ structure, similar to that theoretically predicted by Errandonea and co-workers for AgClO$_4$.[13] As can be seen in the figure, this potential candidate has been found to be energetically noncompetitive for BaCrO$_4$ in the whole pressure range.

From our calculations we have also obtained the elastic constants of BaCrO$_4$. Let us now concentrate on them. For an orthorhombic material there are nine independent elastic constants: C_{11}, C_{22}, C_{33}, C_{44}, C_{55}, C_{66}, C_{12}, C_{13}, and C_{23}. The nine computed elastic constants at equilibrium pressure for the barite-type BaCrO$_4$ structure are collected in Table III, where they are compared with previous theoretical and experimental results on BaCrO$_4$ (Ref. 43) and BaSO$_4$,[44] respectively. As can be seen, the calculated values are in rough agreement and are very close to those experimentally observed in the isostructural BaSO$_4$ compound. The requirements for the Born mechanical stability in orthorhombic structure, i.e.,

$$C_{11} > 0, \quad C_{22} > 0, \quad C_{33} > 0,$$
$$C_{44} > 0, \quad C_{55} > 0, \quad C_{66} > 0,$$
$$(C_{11} + C_{22} - 2C_{12}) > 0, \quad (C_{11} + C_{33} - 2C_{13}) > 0,$$
$$(C_{11} + C_{22} + C_{33} + 2C_{12} + 2C_{13} + 2C_{23}) > 0,$$
$$(C_{22} + C_{33} - 2C_{33}) > 0$$

are fulfilled by our set of elastic constants, pointing out the mechanical stability of the barite BaCrO$_4$ at equilibrium pressure.

According to the Voigt approximation,[45] there is a simple relation between the isotropic bulk modulus B_V and the elastic constants C_{ij}. The computed elastic modulus $B_V = [C_{11} + C_{22} + C_{33} + 2(C_{12} + C_{23} + C_{13})]/9$ is 50.4 GPa and, therefore, consistent with our result from total-energy calculations.

For completeness, we have also calculated three important parameters for further discussion on elasticity. These are the isotropic shear modulus (G), the Young's modulus (E), and the Poisson ratio (υ). The first one is defined as the ratio between stress and strain and is used to provide a measure of the stiffness of a solid. The second one quantifies the stability of the crystal against shear. From the calculated elastic constants in the Voigt method, we can obtain

$$G_v = 1/15[C_{11} + C_{22} + C_{33} + 3(C_{44} + C_{55} + C_{66})$$
$$- (C_{12} + C_{13} + C_{23})] = 24.6 \text{ GPa}.$$

Reuss[46] also suggests a linear relation between the elastic compliance coefficients S_{ij} and the isotropic bulk B_R and the shear G_R moduli,

$$B_R = 1/[S_{11} + S_{22} + S_{33} + 2(S_{12} + S_{13} + S_{23})] = 48.6 \text{ GPa},$$

$$G_R = 15/[4(S_{11} + S_{12} + S_{33}) - 4(S_{12} + S_{13} + S_{23})$$
$$+ 3(S_{44} + S_{55} + S_{66})] = 15.02 \text{ GPa}.$$

However, Hill[47] proved that the Voigt and Reuss equations represent upper and lower limits of the true values. He showed that the bulk modulus B and the shear modulus G can be obtained by the arithmetic mean value: $B_H = B = (B_R + B_V)/2$ and $G_H = G = (G_R + G_V)/2$.

The Young's modulus E and the Poisson ratio υ, can be calculated from the following equations:

$$E_H = (9B_H G_H)/(G_H + 3B_H),$$
$$\upsilon = 1/2[(B_H - (2/3)G_H)/(B_H + (1/3)G_H]$$
$$= (3B_H - 2G_H)/[2(3B_H + G_H)].$$

From our calculated elastic constants we obtain a bulk modulus $B_H = 49.5$ GPa, an isotropic shear modulus $G_H = 19.81$ GPa, a Young's modulus $E_H = 52.43$ GPa, and a Poisson ratio υ_H of 0.32. Since the Poisson ratio $\upsilon = 0.25$ is the lower limit for central force solids and 0.5 is the upper limit, our value indicates that the interatomic forces in this compound are mainly central. Moreover, it should be recalled that the bulk modulus B represents the resistance to fracture, while the shear modulus G represents the resistance to plastic deformation. Thus, if $G/B < 0.5$ the material is considered to behave in a ductile manner, otherwise the materials behave in a brittle manner. Our value of $(G/B)_H = 0.4$ indicates that the crystal is ductile.

The behavior of lattice vibrations under pressure may provide useful information regarding structural instabilities. In this regard, we also report the Raman, infrared, and silent mode phonons at equilibrium pressure and their pressure derivatives for BaCrO$_4$-hashemite.[48–50] According to group-theory analysis, the barite-type BaCrO$_4$ structure displays 36 Raman-active modes corresponding to the following decomposition at the Γ point: $\Gamma = 11A_g + 7B_{1g} + 11B_{2g} + 7B_{3g}$, while the infrared-active modes are 29: $11B_{1u} + 7B_{2u} + 11B_{3u}$. There are also seven silent modes (see Ref. [50]). The Raman modes and their pressure derivatives are in good agreement with the experimental available data.[9,51] No experimental results are available, to our knowledge, for the infrared and silent modes of the hashemite BaCrO$_4$. Finally, we report the Raman and infrared modes of the BaCrO$_4$-$P2_12_12_1$ phase at 16 GPa, and the pressure derivatives.[52] According to group-theory analysis, the Raman- and IR-active modes of the post-barite phase lead to 72 ($\Gamma = 18A + 18B_1 + 18B_2 + 18B_3$) and 54 ($18B_1 + 18B_2 + 18B_3$) modes, respectively, at the zone center, which mean a considerable increase in the number of different lattice vibrations. We hope that this work will stimulate future experiments in this field to cover this lacuna.

In the low-pressure barite-type structure, the sequence of Raman modes very much resembles that of other barite-type oxides. In our case, calculations show that Raman modes for frequencies smaller than 175 cm^{-1} are basically ascribed to the motion of the Ba cation and tetrahedral CrO$_4$ units. The internal vibrations of the CrO$_4$ tetrahedron spanned the frequency range from 341 to 974 cm^{-1} but with a gap between 425 and 905 cm^{-1}. The modes located between 905 and 975 cm^{-1} can be associated with the ν_1 and ν_3 bands of barite. For this structure, the modes with larger pressure coefficients are located between 145 and 175 cm^{-1}. The mode distribution of IR modes is similar to that of Raman, being those with the highest pressure coefficient located from 125 to 190 cm^{-1}. In contrast with Raman modes, there is a soft mode among the IR ones: the B_{1u} mode at 329.18 cm^{-1}.

We have also calculated the Raman and IR modes for the high-pressure phase. Note that the B_1, B_2, and B_3 modes are active for both types of spectroscopy, while the A modes are only Raman active. The increase of the number of vibrations is related to the decrease of the symmetry of the structure induced by the transition. However, still there are many similitudes between the Raman and IR spectra of both phases. In particular, in the HP phase there is also a large phonon gap. In this case the

gap goes from 452 to 933 cm^{-1}. The high-frequency modes are associated to internal bending and stretching vibrations of the CrO$_4$ tetrahedra. In the high-pressure phase, the pressure coefficients are slightly smaller than in the low-pressure phase, but differences are small, which is consistent with the fact that both phases have a similar bulk modulus. In particular, the B_1 mode calculated to be at 281.2 cm^{-1} (at 16 GPa) is the one with the highest pressure coefficient ($d\omega/dP = 4.49$ cm^{-1}/GPa). A noticeable fact is the presence of two soft modes at 320 and 354 cm^{-1} (see Ref. [52]), which suggest that upon further compression the $P2_12_12_1$ phase will become mechanically unstable. The occurrence of a second transition induced by pressure will be the focus of future studies.

In conclusion, the phase transition recently reported for BaCrO$_4$ at high pressures is confirmed. Both x-ray diffraction experiments and *ab initio* total-energy calculations suggest that the high-pressure phase adopts the $P2_12_12_1$ post-barite phase,[11] which is basically a strong distortion of the initial barite phase. The first coordination sphere of the Ba and Cr atoms would not change and only the coordination number of the second sphere would increase from 7 to 8. This transition involves a contraction of the a and c axes of approximately 20% and 3%, respectively, and an expansion of the b axis of approximately 26%. This drastic change in the lattice constants is likely caused by a small displacement and a tilting movement of the [CrO$_4$] tetrahedra, as it occurs in BaSO$_4$.[11] Furthermore, we have found that the onset of the phase transition is highly dependent on the hydrostaticity of the pressure media. Thus, the less hydrostatic the medium, the lower the transition pressure. This new example of post-barite-type structure confirms the location of this structural archetype in the northeast part of the barite-type compounds in the Bastide's diagram. The equations of state of both phases have been determined. We also report the *ab initio* elastic constants for the hashemite phase, showing that the Born stability criteria are fulfilled. Finally we also obtain the Raman, infrared, and silent modes and they pressure derivatives of the low- and high-pressure phases. For both phases all modes are assigned and the most distinctive vibrations described. In particular, for the barite-type phase the agreement with previous experiments is good being several unmeasured modes calculated, which could be an important help for future studies. All Raman and IR modes for the HP phase are also calculated. In this phase we found two soft modes, which suggest that the $P2_12_12_1$ phase will become unstable at pressures higher that those covered by this study.

*Corresponding author.

[1] A. E. Rubin, Meteorit. Planet. Sci. **32**, 231 (1997).

[2] A. Brenier, G. Jia, and C. Tu, J. Phys.: Condens. Matter **16**, 9103 (2002).

[3] M. Kobayashi, M. Ishi, Y. Usuki, and H. Yahagi, Nucl. Instrum. Methods Phys. Res. A **333**, 429 (1993).

[4] M. Nikl, P. Bohacek, E. Mihokova, N. Solovieva, A. Vedda, M. Martini, G. P. Pazzi, P. Fabeni, M. Kobayashi, and M. Ishii, J. Appl. Phys. **91**, 5041 (2002).

[5] M. O'Keeffe and B. G. Hyde, Struct. Bonding (Berlin) **61**, 77 (1985).

[6] D. Santamaría-Pérez and R. Chuliá-Jordán, High Press. Res. **32**, 81 (2012).

[7] A. Vegas, Crystallogr. Rev. **7**, 189 (2000).

[8] W. A. Crichton, M. Merlini, M. Hanfland, and H. Muller, Am. Mineral. **96**, 364 (2011).

[9] T. Huang, S. R. Shieh, A. Akhmetov, X. Liu, C. M. Lin, and J. S. Lee, Phys. Rev. B **81**, 214117 (2010).

[10] P. L. Lee, E. Huang, and S. C. Yu, High Press. Res. **23**, 439 (2003).

[11] D. Santamaría-Pérez, L. Gracia, G. Garbarino, A. Beltrán, R. Chuliá-Jordán, O. Gomis, D. Errandonea, Ch. Ferrer-Roca, D. Martinez-García, and A. Segura, Phys. Rev. B **84**, 054102 (2011).

[12] P. W. Bridgman, Proc. Amer. Acad. Sci. **72**, 207 (1937).

[13] D. Errandonea, L. Gracia, A. Beltrán, A. Vegas, and Y. Meng, Phys. Rev. B **84**, 064103 (2011).

[14] D. Errandonea and F. J. Manjon, Prog. Mater. Sci. **53**, 711 (2008).

[15] R. Lacomba-Perales, D. Errandonea, Y. Meng, and M. Bettinelli, Phys. Rev. B **81**, 064113 (2010).

[16] W. A. Crichton, J. B. Parise, S. M. Antao, and A. Grzechnik, Am. Mineral. **90**, 22 (2005).

[17] L. Gracia, A. Beltrán, D. Errandonea, and J. Andres, Inorg. Chem. **51**, 1751 (2012).

[18] A. P. Hammersley, S. O. Svensson, M. Hanfland, A. N. Fitch, and D. Hausermann, High Press. Res. **14**, 235 (1996).

[19] H. K. Mao, J. Xu, and P. M. Bell, J. Geophys. Res., [Solid Earth and Planets] **91**, 4673 (1986); A. Dewaele, P. Loubeyre, and M. Mezouar, Phys. Rev. B **70**, 094112 (2004).

[20] J. Rodríguez-Carvajal, Physica B **192**, 55 (1993).

[21] G. Nolze and W. Kraus, Powder Diffr. **13**, 256 (1998).

[22] P. Hohenberg and W. Kohn, Phys. Rev. B **136**, 864 (1964).

[23] G. Kresse and J. Furthmuller, Comput. Mater. Sci. **6**, 15 (1996).

[24] G. Kresse and J. Furthmuller, Phys. Rev. B **54**, 11169 (1996).

[25] G. Kresse and J. Hafner, Phys. Rev. B **47**, 558 (1993).

[26] G. Kresse and J. Hafner, Phys. Rev. B **49**, 14251 (1994).

[27] P. E. Blochl, Phys. Rev. B **50**, 17953 (1994).

[28] G. Kresse and D. Joubert, Phys. Rev. B **59**, 1758 (1999).

[29] J. P. Perdew, A. Ruzsinszky, G. I. Csonka, O. A. Vydrov, G. E. Scuseria, L. A. Constantin, X. L. Zhou, and K. Burke, Phys. Rev. Lett. **100**, 136406 (2008).

[30] A. Mujica, A. Rubio, A. Munoz, and R. J. Needs, Rev. Mod. Phys. **75**, 863 (2003).

[31] N. Chetty, A. Munoz, and R. M. Martin, Phys. Rev. B **40**, 11934 (1989).

[32] S. Baroni, S. de Gironcoli, A. Dal Corso, and P. Giannozzi, Rev. Mod. Phys. **73**, 515 (2001).

[33] K. Parlinski, Z.-Q. Li, and Y. Kawazoe, Phys. Rev. Lett. **78**, 4063 (1997); K. Parlinski, Computer code PHONON, Cracow, 2008.

[34] O. Beckstein, J. E. Klepeis, G. L. W. Hart, and O. Pankratov, Phys. Rev. B **63**, 134112 (2001).

[35] J. F. Nye, *Physical Properties of Crystals. Their Representation by Tensor and Matrices.* (Oxford University Press, New York, 1957).

[36] E. N. Duesler and E. E. Foord, Am. Mineral. **71**, 1217 (1986).

[37] A. Lentz, W. Buchele, and H. Schollhorn, Cryst. Res. Technol. **21**, 827 (1986).

[38] D. Errandonea, Y. Meng, M. Somayazulu, and D. Hausermann, Physica B **355**, 116 (2005).

[39] J. Ruiz-Fuertes, D. Errandonea, R. Lacomba-Perales, A. Segura, J. González, F. Rodríguez, F. J. Manjón, S. Ray, P. Rodríguez-Hernández, A. Muñoz, Z. Zhu, and C.Y. Tu, Phys. Rev. B **81**, 224115 (2010).

[40] E. Bandiello, D. Errandonea, D. Martinez-Garcia, D. Santamaria-Perez, and F. J. Manjón, Phys. Rev. B **85**, 024108 (2012).

[41] Y. W. Long, L. X. Yang, S. J. You, Y. Yu, R. C. Yu, C. Q. Jin, and J. Liu, J. Phys.: Condens. Matter **18**, 2421 (2006).

[42] D. Errandonea, R. S. Kumar, S. N. Achary, and A. K. Tyagi, Phys. Rev. B **84**, 224121 (2011).

[43] U. Becker, P. Risthaus, F. Brandt, and D. Bosbach, Chem. Geol. **225**, 244 (2006).

[44] C. Schaefer, L. Bergmann, E. Fues, and H. Ludloff, Sitzber. Preuss. Akad. Wiss. Phys.-Math. Kl. **1935**, 222 (1935).

[45] W. Voigt, *Lehrbuch der Kristallphysik* (Verlag und Druck, Leipzig und Berlin, 1928).

[46] Z. Reuss, Angew. Math. Mech. **9**, 49 (1929).

[47] R. Hill, Proc. Phys. Soc. London, Sect. A **65**, 349 (1952).

[48] See Supplemental Material at http://link.aps.org/supplemental/10.1103/PhysRevB.86.094116 for Raman mode phonons at equilibrium pressure of $BaCrO_4$-hashemite and their pressure derivatives.

[49] See Supplemental Material at http://link.aps.org/supplemental/10.1103/PhysRevB.86.094116 for infrared mode phonons at equilibrium pressure of $BaCrO_4$-hashemite and their pressure derivatives.

[50] See Supplemental Material at http://link.aps.org/supplemental/10.1103/PhysRevB.86.094116 for silent mode phonons at equilibrium pressure of $BaCrO_4$-hashemite and their pressure derivatives.

[51] D. Wallace and H. Callen, *Thermodynamics of Crystals* (Dover, New York, 1998).

[52] See Supplemental Material at http://link.aps.org/supplemental/10.1103/PhysRevB.86.094116 for Raman and infrared modes of the $BaCrO_4$-$P2_12_12_1$ phase at 16 GPa, and the pressure derivatives.